Mathematical Biosciences and Engineering

MBE, 21(2): 3207–3228.
DOI: 10.3934/mbe.2024142
Received: 18 December 2023
Revised: 09 January 2024
Accepted: 21 January 2024
Published: 01 February 2024

https://www.aimspress.com/journal/MBE

Research article

Deterministic and stochastic approaches to a minimal model for the transition from autophagy to apoptosis

Bojie Yang and Zhuoqin Yang*

School of Mathematical Sciences, Beihang University, Beijing 100191, China

* **Correspondence:** Email: yangzhuoqin@buaa.edu.cn.

Abstract: Autophagy and apoptosis are crucial cellular mechanisms. The cytoprotective function of autophagy is mediated by the negative regulation of apoptosis, which in turn inhibits autophagy. Although research into the molecular connection between autophagy and apoptosis is booming, the intricate regulatory mechanisms of this process are still not completely understood. Therefore, the objective of this study was to develop a minimal model to explore the transition from autophagy to apoptosis. This biological system was analyzed by comprehensively integrating both the deterministic and the stochastic dynamics of the cells. The system exhibited bistability, and the statistical properties of cells undergoing autophagy and apoptosis were analyzed at two different stress levels with varying noise strengths. Moreover, we investigated how noise affected the double negative feedback loops between autophagy and apoptosis and further triggered transitions at two different stress levels and initial conditions. Finally, the effect of noise on transition was comprehensively studied under continuous stress variations and the two different initial conditions, showing that stronger noise results in more randomness during the switching process. Our work may provide novel insights for further experiments and modeling.

Keywords: autophagy; apoptosis; bifurcation; stochastic; noise

1. Introduction

Autophagy is an evolutionarily conserved cellular degradation mechanism that maintains intracellular homeostasis [1,2]. Unnecessary or dysfunctional cellular organelles and proteins are sequestered in vesicles and delivered to the lysosome for digestion and recycling [3,4]. Under tolerable

stress conditions, such as nutrient starvation or growth factor withdrawal, autophagy functions in a "self-eating" role to protect cells; by contrast, severe or sustained stress stimulates a "self-killing" process known as apoptosis, a genetically programmed form of cell death that eliminates cells during embryonic development and immune system maturation [5,6]. Apoptotic cell death is governed by two basic rules: 1) weak stress signals cannot trigger the apoptosis response; and 2) cells undergo death once apoptosis has been initiated. Thus, there is a distinct borderline between two well-separated cell states, survival and death, i.e., the state of on autophagy and off apoptosis and that of off autophagy and on apoptosis [7–9].

The crosstalk between autophagy and apoptosis is highly complex, especially on a molecular level [10–12]. Accumulating evidence indicates that these two processes are not independent of each other but influence each other through common pathways [10,13,14]. Typically, there are three groups of regulators of the network, i.e., autophagy inducers, apoptosis inducers and crosstalk elements. The autophagy inducers, such as Beclin1 (the mammalian homolog of yeast Atg6) [15] and AMBRA1 [16], promote cell survival [17], while the crucial inducer of apoptosis is Caspases, typically involving the activation of a family of cysteine proteases [18,19]. It has been shown that Bcl2 [20,21], p53 [22], mTOR [23], Calpain [24] and Ca^{2+} [25] act as crosstalk elements and are involved in regulating both autophagy and apoptosis pathways.

The complex biological process based on both experimental and theoretical considerations has been studied by several mathematical models [6,26–28]. For example, in our previous work, we found that binding of B-cell lymphoma-2 (Bcl2) family proteins to AMBRA1 in endoplasmic reticulum and mitochondria regulated the switch from autophagy to apoptosis under the two different types of stress [28]. The mathematical model proposed by Kapuy et al. [6] contained three parts with crosstalk elements, with autophagy and apoptosis inducers involved in feedback loops. The modeling studies have considered molecular interaction pathways and included a detailed analysis of specific biological processes of the crosstalk between autophagy and apoptosis.

The above models have integrated the whole complex system rather than focusing on the crucial double negative feedback loops between autophagy and apoptosis. Herein, we strive to minimize the model and highlight the double negative feedback loops under stress. Numerous studies [6,27–29] have shown that stress stimuli trigger the parallel induction of Beclin1-induced autophagy and Caspases-dependent apoptosis; therefore, the element of crosstalk between Bcl2 and pro-apoptotic protein Bax is not considered here. Besides, the process by which the inactive form of Beclin1 promotes the activation of Caspases can be neglected when the mutual inhibition between the active form of Beclin1 and Caspases is considered [30]. Therefore, we propose a minimal model, i.e., stress stimulates both Beclin1-dependent autophagy and Caspases-mediated apoptosis, and we verified that the minimal model reproduces the results of the original model [6].

The network consisting of the double negative feedback loops between autophagy and apoptosis can be solved mathematically to find deterministic steady-state solutions. The deterministic simulations can be used to find the bistable switch from autophagy to apoptosis. In addition, it is well known that noise commonly exists in biological systems owing to internal and external environmental fluctuations [31–33]. It is important to include noise to obtain realistic results with stochastic simulations [34,35]. Deterministic simulations are commonly used to study the dynamical behaviors of individual cells, whereas stochastic simulations are generally well-suited to studies of the population behavior of cells [29]. Therefore, in this work, we study the dynamical transition from autophagy to apoptosis under stimulation of stress by means of both deterministic and stochastic simulations.

We exhibit the biostability of the system under two different levels of stress and analyze the statistical properties of cells that undergo autophagy and apoptosis under two different initial conditions with varying noise strengths. Moreover, under two different levels of stress and different initial conditions, we investigate how noise affects the double negative feedback loops between autophagy and apoptosis. Finally, the effect of noise on the transition is comprehensively explored by means of bifurcation and statistical analysis under continuous changes in stress and the two different initial conditions. For different stresses and initial conditions, we find that stronger noise induces more randomness in the switching process. These results enhance our understanding of the interaction mechanism between autophagy and apoptosis and provide new insights for further dynamical modeling.

2. Materials and methods

The minimal mathematical model (Figure 1) shows the key structures of stress-induced Beclin1-dependent autophagy and Caspases-mediated apoptosis. The existing antagonistic relationships between Beclin1 and Caspases form the double negative feedback loops. Based on the biochemical interactions, we describe the dynamics of the crosstalk between Beclin1 ($[B]$) and Caspases ($[C]$) under stress (S) using ordinary differential equations (1) and (2), which are solved via Runge-Kutta [36] methods for very high precision.

$$\frac{d[B]}{dt} = \frac{(k_1+k_2\cdot S)\cdot(Bt-B)}{(Jbe+Bt-B)} - \frac{(k_3+k_4\cdot C)\cdot B}{(Jbe+B)} \tag{1}$$

$$\frac{d[C]}{dt} = \frac{(k_5+k_6\cdot S)\cdot(Ct-C)}{(Jcp+Ct-C)} - \frac{(k_7+k_8\cdot B)\cdot C}{(Jcp+C)} \tag{2}$$

The first term in Eq (1) corresponds to the basal and stress-dependent activation of Beclin1, and the second term corresponds to its basal and Caspases-dependent deactivation. Equation (2) represents the dynamics of Caspases and has two terms: basal and stress-dependent activation, and basal and Beclin1-dependent inactivation. The terms $\xi_1(t)$ and $\xi_2(t)$ are added to Eqs (1) and (2), respectively, to represent Gaussian white noise with zero mean and an auto-correlation function, where $<\xi_1(t)\xi_1(s)>= 2D_1\delta(t-s)$, $<\xi_2(t)\xi_2(s)>= 2D_2\delta(t-s)$. Here, we consider the identical noise strengths $D_1 = D_2 = D$. All parameters used in the model and their descriptions are displayed in Table 1.

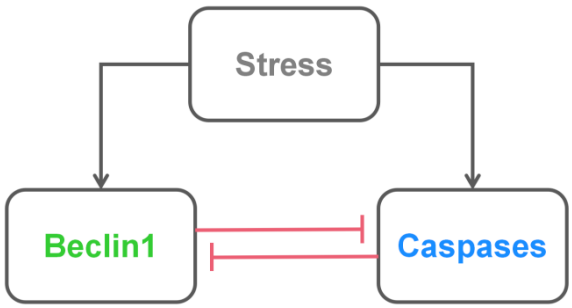

Figure 1. Schematic representation of a minimal network of stress-induced autophagy and apoptosis, where promotion and inhibition are denoted by solid lines with arrowheads and blocked-end lines, respectively.

The model was used in numerical simulations to explore the qualitative dynamic behaviors of the system. All the bifurcation diagrams were analyzed with XPPAUT software [36], and the simulations were performed using Matcont software [37].

Table 1. Parameters and descriptions.

Parameter	Significance	Value	Unit
S	Stress level	1	–
k_1	Basal activation rate constant of Beclin1	2	h^{-1}
k_2	Stress-dependent activation rate constant of Beclin1	0.1	h^{-1}
k_3	Basal inactivation rate constant of Beclin1	0.01	h^{-1}
k_4	Caspases-dependent inactivation rate constant of Beclin1	4	h^{-1}
k_5	Basal activation rate constant of Caspases	0.31	h^{-1}
k_6	Stress-dependent activation rate constant of Caspases	0.1	h^{-1}
k_7	Basal inactivation constant of Caspases	0.1	h^{-1}
k_8	Beclin1-dependent inactivation rate constant of Caspases	0.37	h^{-1}
Jbe	Michaelis constant of Beclin1	0.7	μM
Jcp	Michaelis constant of Caspases	0.01	μM
Bt	Total level of Beclin1	1	μM
Ct	Total level of Caspases	1	μM

3. Results

3.1. Deterministic and stochastic properties under two different levels of stress

Stress as a switch triggers Beclin1-dependent autophagy and Caspases-mediated apoptosis in the molecular network. In this section, we explore the dynamic behaviors of interactions between cell survival and death under small and large stress conditions, respectively.

3.1.1. Stability analysis of the system

The time series of $[B]$ and $[C]$ initiated at values in [0, 1] under small ($S = 1$) and large sustained ($S = 2$) stresses in the deterministic system are displayed in Figure 2A1,B1, respectively. Here, we employ the same initial ranges [0, 1] of $[B]$ and $[C]$ to confirm their final opposite steady state concentrations. Under $S = 1$, $[B]$ ($[C]$) reaches a low (high) level at large initial values but a high (low) level at small initial values. Under $S = 2$, [B] decreases to a low level after transient activation, whereas [C] increases to a high level after transient inactivation. Indeed, two stable steady state levels exists under the small stress $S = 1$ but only one under the large stress $S = 2$.

Two nullclines of $[B]$ and $[C]$ were computed by setting $d[B]/dt = 0$ and $d[C]/dt = 0$ in the phase planes (Figure 2A2,B2). The two nullclines under small stress $S = 1$ intersected at one unstable state (gray) and two stable states (dark), as shown in Figure 2A2. In addition, the vector field (indicated by small arrows) for $S = 1$ indicated that the trajectory moved from the unstable state,

probably to either of the two stable states. These bistable results under $S = 1$ demonstrate that the system eventually stays at either of the two stable states, i.e., at a high level of $[B]$ or of $[C]$, such that autophagy and apoptosis cannot coexist in a cell.

The two nullclines under the large, sustained stress $S = 2$ intersected at only one stable state (dark) for the low $[B]$ level but high $[C]$ level (Figure 2B2). All small arrows in the vector field were directed to the stable point. The monostable steady state for the high $[C]$ level under this stress implies that large and intolerable stress turns off autophagy and ultimately leads to apoptosis.

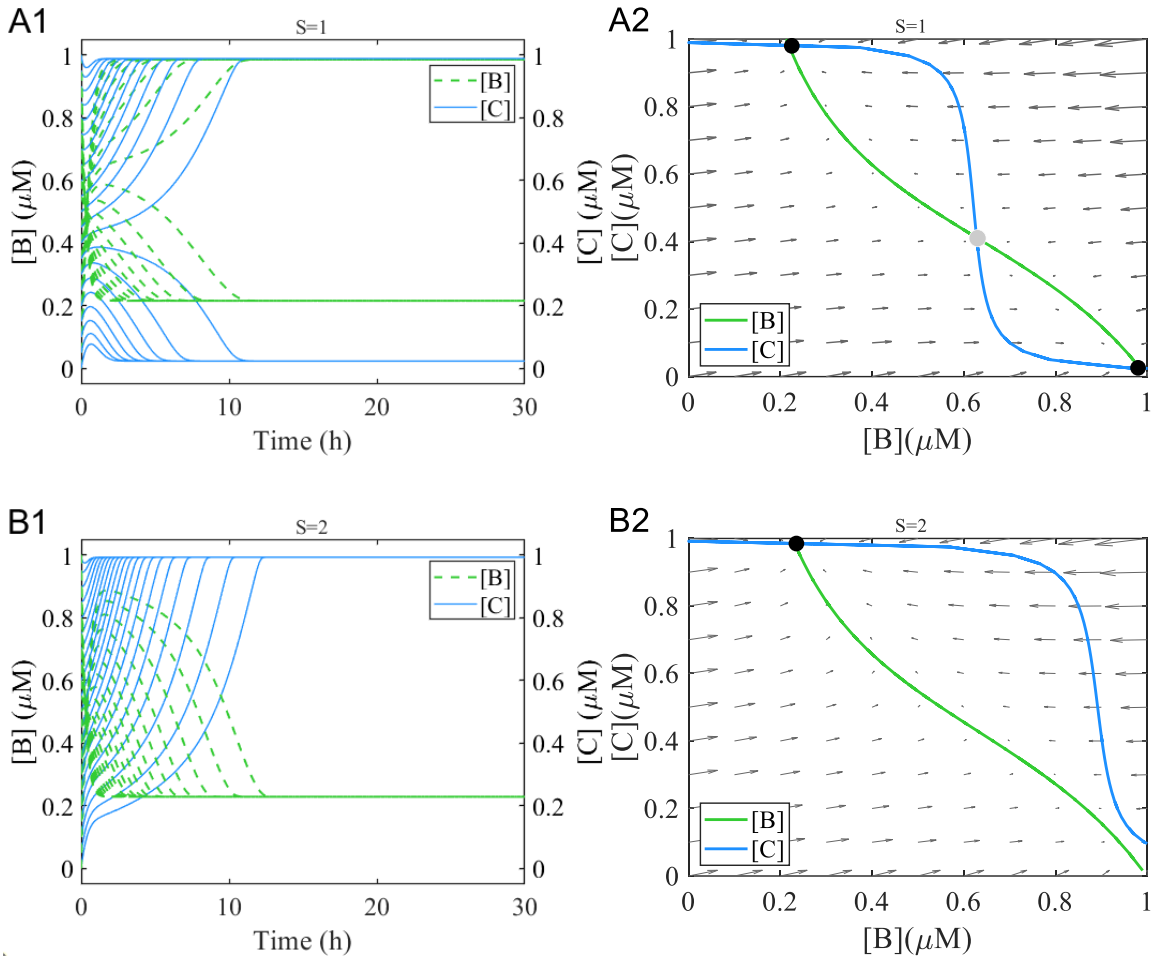

Figure 2. Temporal dynamics and two nullclines with vector fields for Beclin1 ($[B]$) and Caspases ($[C]$) under two different levels of stress, $S = 1$ (A) and $S = 2$ (B). Gray arrows denote the vector field, and the stable and unstable steady states are indicated by black and gray solid circles, respectively.

3.1.2. Statistical properties of cells with respect to autophagy and apoptosis in the presence of noise

Noise resulting from both internal stochastic behaviors and external environmental perturbations is ubiquitous in biological systems and has been extensively studied from both theoretical and experimental perspectives [31,32,34]. As the behavior of a single cell may not be representative, we considered population behaviors of cells in making decisions between autophagy and apoptosis.

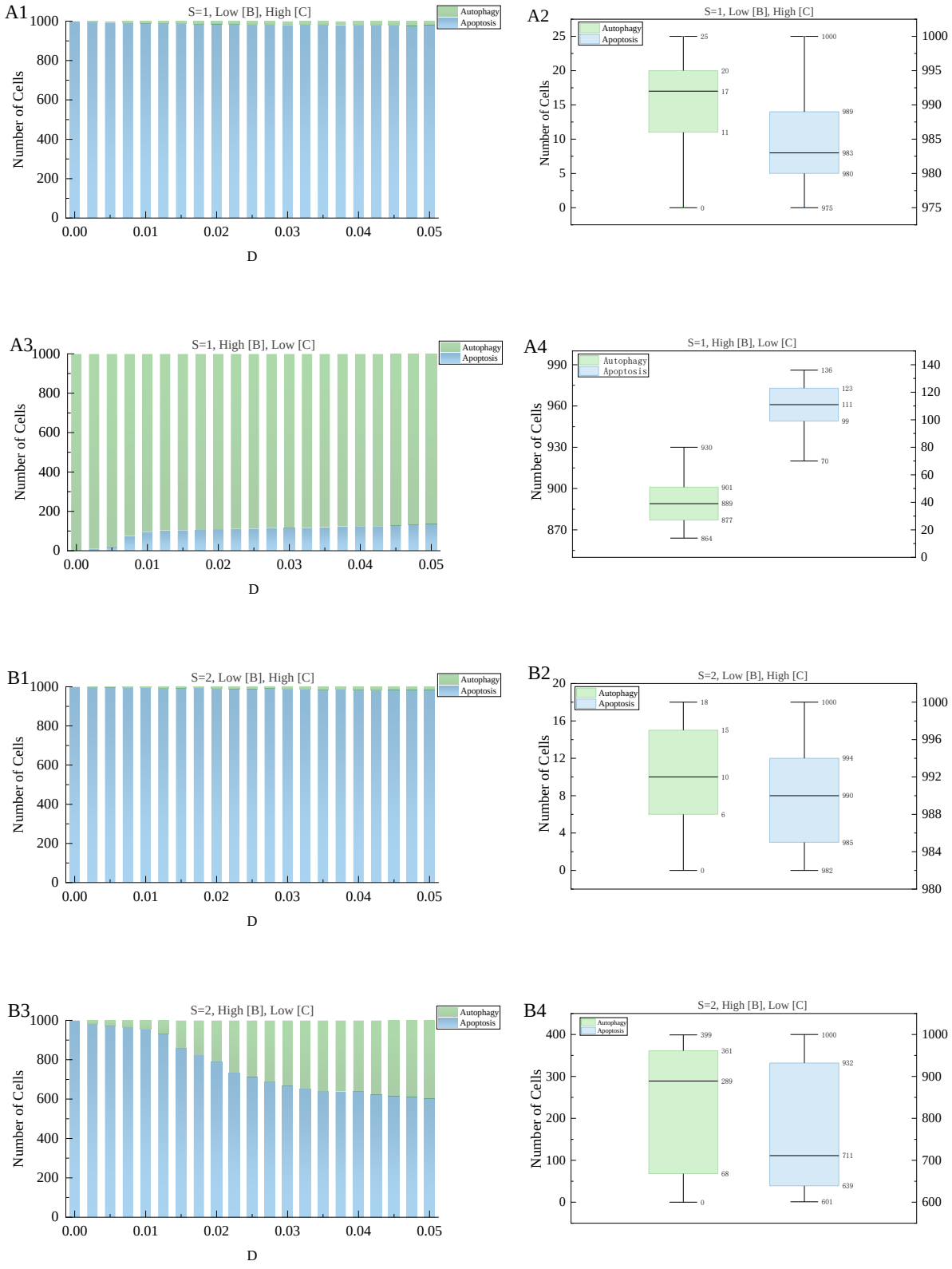

Figure 3. Distributions of cells undergoing autophagy and apoptosis with noise under different levels of stress, $S = 1$ (A) and $S = 2$ (B). Histograms of different values of noise intensity D for each bar were calculated at $t = 30$ h, and the boxplots were calculated using the histograms from the three data sets.

As shown in Figure 3, we investigated statistical characteristics of cells with respect to autophagy and apoptosis using Eqs (1) and (2) with the noise term ($\xi_i, i = 1, 2$). We performed 1000 runs as one dataset, represented in the histograms, to describe the population behavior of 1000 cells with respect to autophagy (green) or apoptosis (blue), with the noise intensity D ranging from 0.001 to 0.05. Then, we calculated the average of three datasets for all values of D and displayed the results in boxplots, including an upper edge, upper quartile, median, lower quartile, and lower edge.

Here, we aimed at bistability when $S = 1$ (Figure 3A) and monostability when $S = 2$ (Figure 3B), by setting two different initial conditions: low $[B]$ but high $[C]$ (first row in Figure 3A,B); and high $[B]$ but low $[C]$ (second row in Figure 3A,B).

Under stress $S = 1$ (Figure 3A), the number of apoptotic cells (blue) was much larger than the number of autophagy cells (green) after initiation with low $[B]$ but high $[C]$, whereas the reverse was observed after initiation with high $[B]$ but low $[C]$. As D increased, the number of apoptotic cells decreased under low $[B]$ but high $[C]$ initial conditions, whereas it increased under high $[B]$ but low $[C]$ conditions. It was worth noting that the initial concentrations with the low $[B]$ but high $[C]$ do not always arrive at the same final steady-state concentrations under disturbance of the noise term. Most of the 1000 cells in a population tend to apoptosis while a few cells affected by noise arrive at their final steady-state with the high $[B]$ but low $[C]$ for autophagy, as seen in Figure 3A1,B1.

Under $S = 2$ (Figure 3B), the number of apoptotic cells (blue) was always much larger than the number of autophagic cells (green), for both low $[B]$ but high $[C]$ and high $[B]$ but low $[C]$ initial conditions. As D increased, the number of apoptotic cells decreased for both sets of initial conditions.

The lengths of the boxes in the boxplots, representing the dispersion of the datasets, suggest that the distribution of cells at smaller S was more concentrated. This demonstrates that smaller stress leads to less fluctuation in the biosystem compared to a larger stress.

Bistability under the small stress and monostability under large stress in (Subsection 3.1.1) were responsible for the population behaviors of the autophagy and apoptotic cells for the two different sets of initial conditions $[B]$ and $[C]$; these were different under the small stress but identical under large stress. Moreover, an increase in noise intensity disturbed the population behaviors, potentially also affecting the choice between cell survival and death.

3.2. Stochastic switch between autophagy and apoptosis modulated by parameters k_4 and k_8

Mutual inhibition between Beclin1-induced autophagy and Caspases-dependent apoptosis determines decision between life and death [6]. Thereby, we further altered the values of two key parameters, k_4 (Caspases-dependent inactivation rate constant of Beclin1) and k_8 (Beclin1-dependent inactivation rate constant of Caspases), to investigate the stochastic switch between autophagy and apoptosis under the two different stresses $S = 1$ and 2.

The bistable behavior under small stress $S = 1$ was located at the basal value of $k_4 = 4$. We further constructed bifurcation diagrams of the steady state levels of $[B]$ and $[C]$ as a function of k_4 as shown in Figure 4A,B, respectively. The bistability of the low and high stable steady states (solid lines) separated by the unstable steady states (dashed lines) still covered a relatively large range of k_4 between the two fold points F_1 and F_2.

We focused on the switch from autophagy to apoptosis by calculating the ratio of the number of apoptotic cells to all 1000 cells, F_t, for the parameter k_4 at D=0.001 (orange), 0.005 (gray), and 0.01 (purple) (Figure 5). Here, we still considered the two different initial conditions of low $[B]$ but high

[C] (Figure 5A) and high $[B]$ but low $[C]$ (Figure 5B). Under the initial condition of low $[B]$ but high $[C]$ (Figure 5A), the F_t curves were more affected by the noise intensity D at smaller values of k_4. As k_4 grew large, the F_t curves were robust to D. Therefore, the fold point F_2 from monostability to bistability, as shown in Figure 4A, affected the sensitivity to noise of the switch from autophagy to apoptosis; in particular, at $k_4 = 2.2$, near the critical point of the switch from autophagy to apoptosis, the F_t values for D = 0.001, 0.005, and 0.1 were 3, 10 and 25%, respectively (Figure 5A). Under the initial condition of high $[B]$ but low $[C]$ (Figure 5B), D had a greater influence on F_t at moderate values of k_4. For example, at $k_4 = 10$, the values of F_t were 0, 1 and 33% as D increased from 0.001 to 0.005 and then to 0.1, respectively.

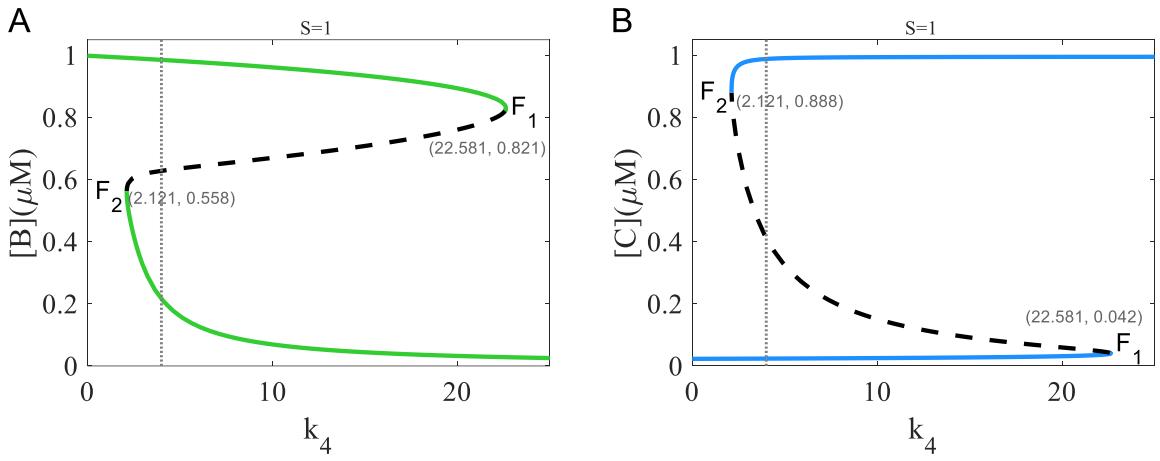

Figure 4. Bifurcation diagrams for Beclin1 (A) and Caspases (B) under $S = 1$ for the parameter k_4. The stable and unstable steady states are represented by solid and black dotted lines, respectively, and F_1 and F_2 are the fold bifurcation points. The gray dotted lines represent the fixed value of $k_4 = 4$ in Table 1. The gray dotted lines represents the fixed value of k_4.

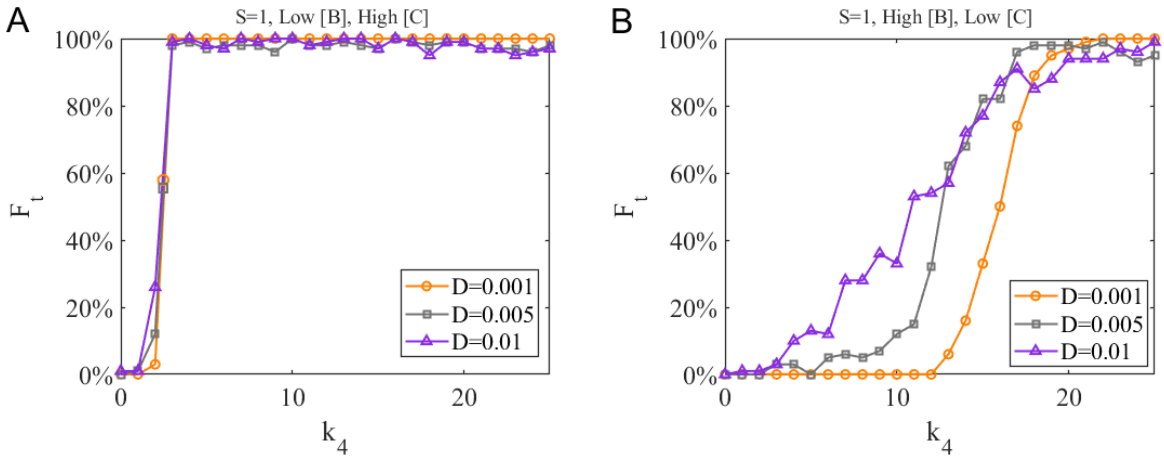

Figure 5. Stochastic behaviors of the cell population under $S = 1$ regulated by the parameter k_4 under conditions of low Beclin1 but high Caspases (A) and high Caspases but low Beclin1 (B). F_t is the ratio of transiting cells to all cells and as a function of k_4 for different values of D.

The bistability under large stress $S = 2$ was also located at the basal value of $k_4 = 4$. Furthermore, we plotted bifurcation diagrams of the steady state levels of $[B]$ and $[C]$ as a function of k_4 for $S = 2$ (Figure 6A,B, respectively). Unexpectedly, bistability appeared within a small range of k_4 between the two fold points F_1 and F_2.

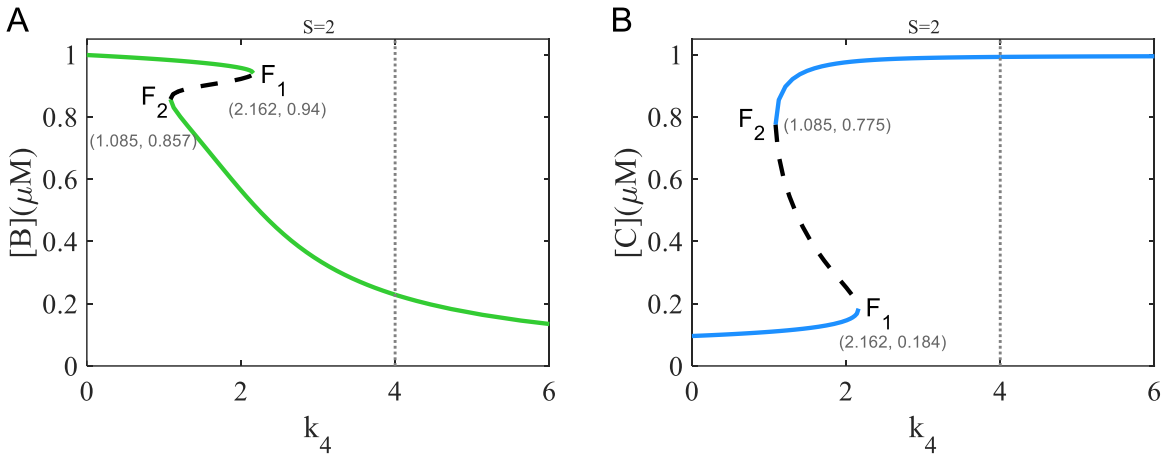

Figure 6. Bifurcation diagrams for Beclin1 (A) and Caspases (B) under $S = 2$ for the parameter k_4. The stable and unstable steady states are represented by solid and black dotted lines, respectively, and F_1 and F_2 are the fold bifurcation points. The gray dotted lines represent the fixed value of $k_4 = 4$ in Table 1.

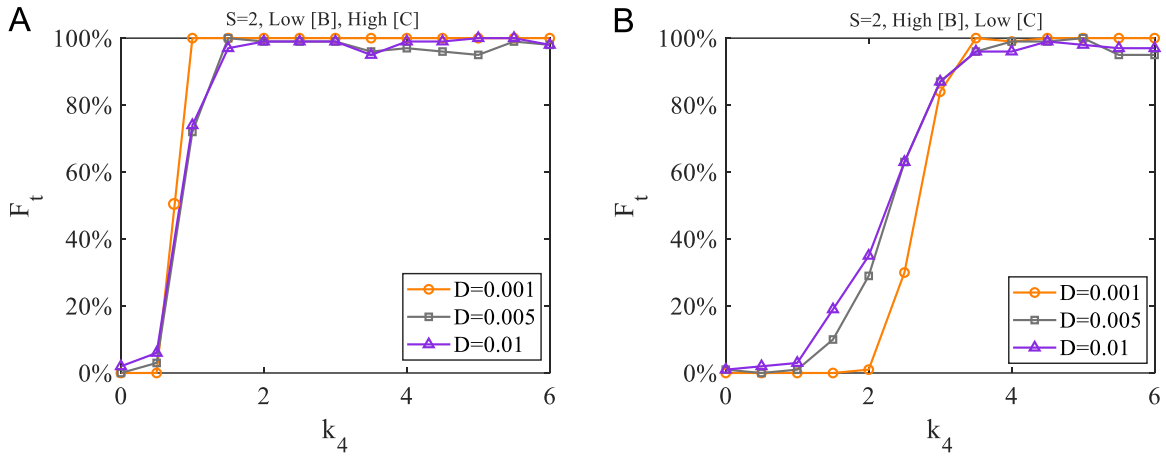

Figure 7. Stochastic behaviors of the cell population under $S = 2$ regulated by the parameter k_4 under conditions of low Beclin1 but high Caspases (A) and high Caspases but low Beclin1 (B). F_t is the ratio of transiting cells to all cells and as a function of k_4 for different values of D.

Under the condition of low $[B]$ but high $[C]$ (Figure 7A), the F_t curves were more affected by D in the bistable range of k_4. We picked a key point for the switch at $k_4 = 1.1$ to achieve changes in F_t from 100 to 81% and then to 80%, with D increasing from 0.001 to 0.005 and then to 0.01. Under the condition of high $[B]$ but low $[C]$ (Figure 7B), the F_t curves showed more fluctuation with changes in D in the bistable range of k_4. For example, at $k_4 = 2$, as D increased from 0.001 to 0.005

to 0.1, the F_t values were 0, 29 and 35%, respectively.

The situation was quite different under the regulation of k_8. Under small stress $S = 1$, the bistable behavior was calculated at the basal value of $k_8 = 0.37$. The bifurcation diagrams of the steady state levels of $[B]$ and $[C]$ as a function of k_8 are plotted in Figure 8A,B, respectively. The bistability of the low and high stable steady states (solid lines) separated by the unstable steady states (dashed lines) covered a small range of k_8 between the two fold points F_1 and F_2.

Under the condition of low $[B]$ but high $[C]$, the F_t curves were more affected by the noise intensity D in the bistable range of k_8 (Figure 9A1). The key point for the switch to happen was $k_8 = 0.8$; as D changed from 0.001 to 0.005 and 0.1, the F_t values were 92, 53 and 49%, respectively. Under the condition of high $[B]$ but low $[C]$ (Figure 9B1), the F_t curves were affected more by D in the bistable range of k_8. For example, at $k_8 = 0.3$, F_t took values of 0, 3, and 30% as D increased from 0.001 to 0.005 and then to 0.1, respectively.

In addition, under large stress $S = 2$, monostability was observed at the basal value of $k_8 = 0.37$. However, as shown in the bifurcation diagrams of the steady state levels of $[B]$ and $[C]$ as a function of k_8 (Figure 10A,B, respectively), bistability also emerged within a small range of k_8 between the two fold points F_1 and F_2.

Under the condition of low [B] but high $[C]$, the F_t curves were affected more by D in the bistable range of k_8 (Figure 11A). At the key point for the switch, $k_8 = 1.1$, F_t changed from 98 to 54% and then to 46% with D values of 0.001, 0.005, and 0.01, respectively. Under the condition of high $[B]$ but low $[C]$, the F_t curves showed more fluctuation with changes in D in the bistable range of k_8 (Figure 11B1). For example, at $k_8 = 0.45$, the F_t values were 0, 28 and 35%, as D increased from 0.001 to 0.005 and then to 0.1, respectively.

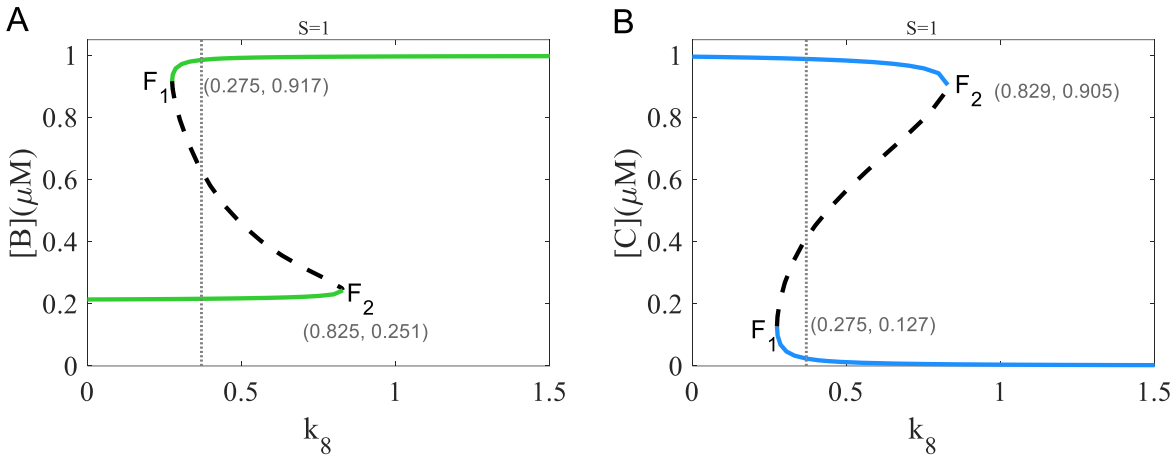

Figure 8. Bifurcation diagrams for Beclin1 (A) and Caspases (B) under $S = 1$ for the parameter k_8. The stable and unstable steady states are represented by solid and black dotted lines, respectively, and F_1 and F_2 are the fold bifurcation points. The gray dotted lines represent the fixed value of $k_8 = 0.37$ in Table 1.

Under the condition of low [B] but high $[C]$, the F_t curves were affected more by D in the bistable range of k_8 (Figure 11A). At the key point for the switch, $k_8 = 1.1$, F_t changed from 98 to 54% and then to 46% with D values of 0.001, 0.005, and 0.01, respectively. Under the condition of high $[B]$ but low $[C]$, the F_t curves showed more fluctuation with changes in D in the bistable range of

k_8 (Figure 11B1). For example, at $k_8 = 0.45$, the F_t values were 0, 28 and 35%, as D increased from 0.001 to 0.005 and then to 0.1, respectively.

Taken together, these findings indicate that for both small and large stresses, the regulation of k_4 or k_8 guarantees bistability, with threshold values for the switch from autophagy to apoptosis. Moreover, the two parameters k_4 (Caspases-dependent inactivation rate constant of Beclin1) and k_8 (Beclin1-dependent inactivation rate constant of Caspases) had opposite regulatory effects on the transition from autophagy to apoptosis.

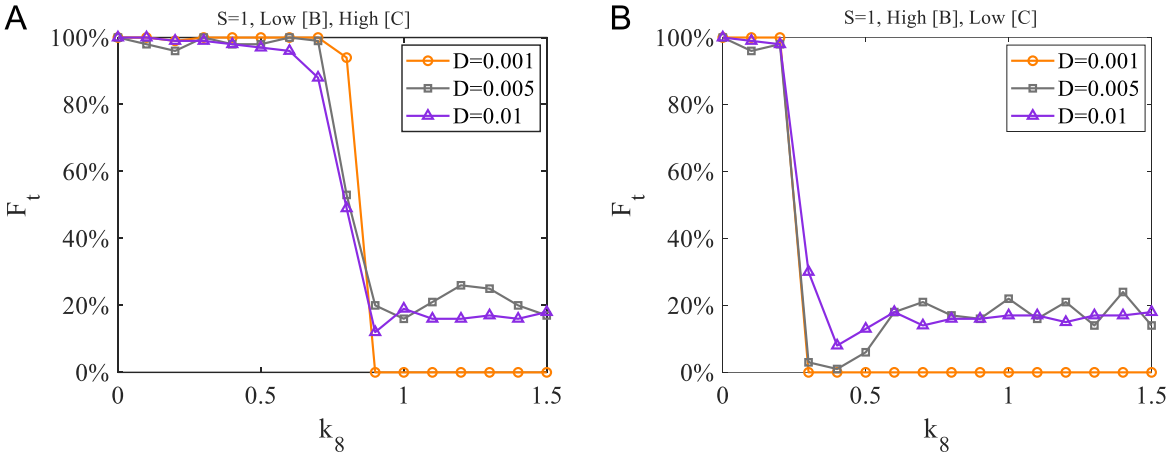

Figure 9. Stochastic behaviors of the cell population under $S = 1$ regulated by the parameter k_8 under conditions of low Beclin1 but high Caspases (A) and high Caspases but low Beclin1 (B). F_t is the ratio of transiting cells to all cells and as a function of k_8 for different values of D.

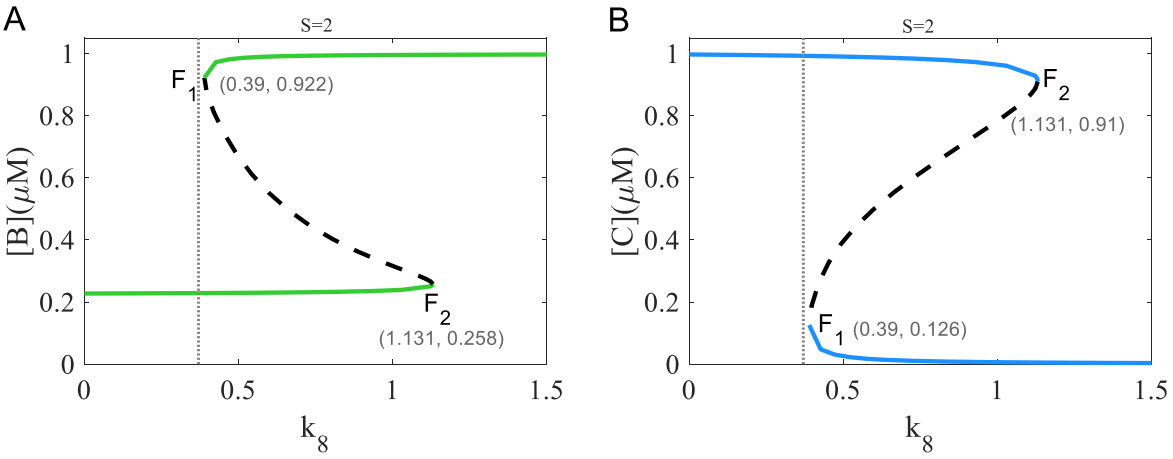

Figure 10. Bifurcation diagrams of Beclin1 (A) and Caspases (B) under $S = 2$ for the parameter k_8. The stable and unstable steady states are represented by solid and black dotted lines, respectively, and F_1 and F_2 are the fold bifurcation points. The gray dotted lines represent the fixed value of $k_8 = 0.37$ in Table 1.

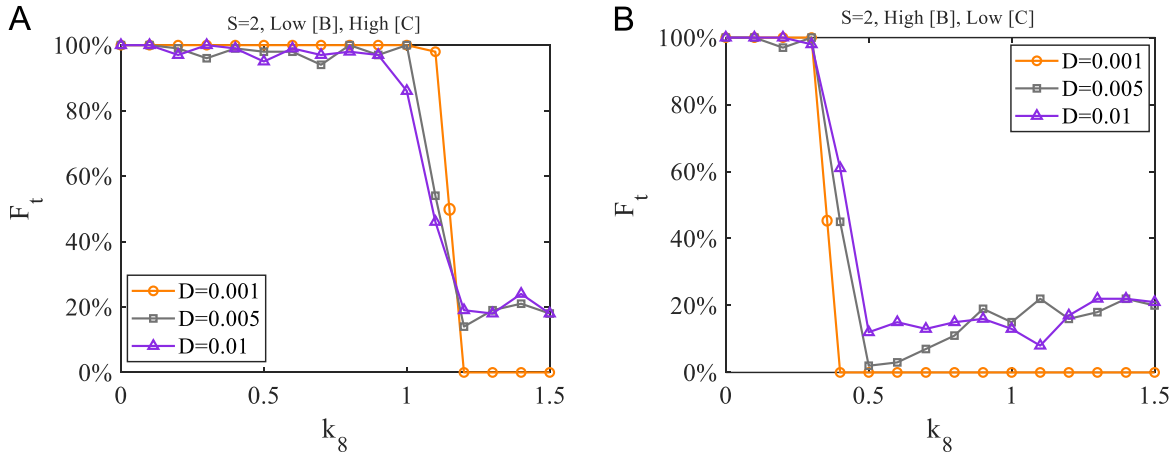

Figure 11. Stochastic behaviors of the cell population under $S = 2$ regulated by the parameter k_8 under conditions of low Beclin1 but high Caspases (A) and high Caspases but low Beclin1 (B). F_t is the ratio of transiting cells to all cells and as a function of k_8 for different values of D.

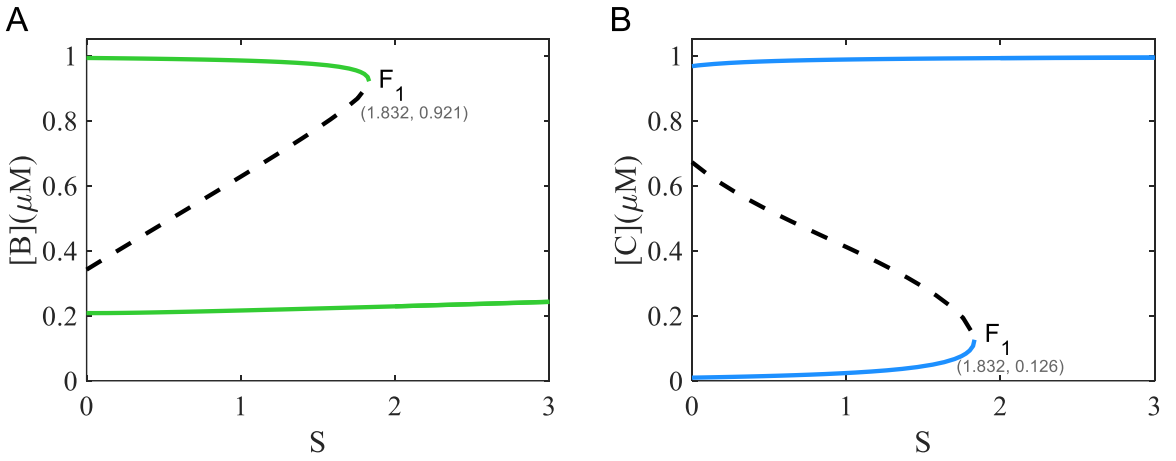

Figure 12. Bifurcation diagrams for Beclin1 (A) and Caspases (B), respectively. The stable and unstable steady states are represented by solid and black dotted lines, respectively, and F_1 and F_2 are the fold bifurcation points.

3.3. Deterministic and stochastic properties with varying stress

In the above section, we discussed the effects of two discrete and different stresses on the switch from autophagy to apoptosis with varying levels of noise. Here, we explore the transition under continuous stress from both deterministic and stochastic perspectives.

3.3.1. Response of the bistable switches to noise stimuli

It has been shown that both $[B]$ and $[C]$ reach their bistable steady states under small stress $S = 1$ (Figure 2). Here, we further explore the dynamic properties of $[B]$ and $[C]$ as a function of S through bifurcation analysis. In Figure 12, the low and high stable steady states (solid lines) are

separated by unstable steady states (dashed lines) located between the two-fold points F_1 and F_2 on "Z"-shaped and "S"-shaped bifurcation curves of $[B]$ and $[C]$, respectively. The results reproduce the dynamic transitions observed in [6]. From a biological perspective, it is important to consider the division of the positive half axis of $(S,[B])$- and $(S,[C])$-planes. The irreversible bistable switch results from the fold point F_2 located in the negative half of the stress axis. Therefore, the low (or high) stable state fails to transit to the high (or low) stable state as S decreases. Biologically, when S reaches a threshold value, Beclin1 is deactivated (or Caspases are activated), so the cells cannot survive but will undergo apoptosis.

Under the condition of low $[B]$ but high $[C]$ (Figure 13A1), the F_t curve reaches nearly 100% with variations in S for *D* fixed at 0.001, 0.005, or 0.1. The three scatter plots in Figure 13A2 show increasing *D* (from top to bottom) at $S = 1.7$, and the green and blue dots represent autophagic and apoptotic cells, respectively. Almost all cells remained at the stage of apoptosis; however, larger values of *D* resulted in more cells undergoing autophagy and a more discrete distribution of cells. Under the condition of high $[B]$ but low $[C]$ (Figure 13B1), the F_t curves were affected more by *D* in the bistable range of S. For example, at $S = 1.7$, F_t took values of 6, 46 and 57% as *D* increased from 0.001 to 0.005 and then to 0.1, respectively. The three scatter plots with increasing *D* (from top to bottom) at $S = 1.7$ in Figure 13B2 show much more autophagy than apoptosis. As *D* increases, more and more cells transition from autophagy to apoptosis, and the distribution of cells becomes more discrete. These results imply that for a given level of stress, the initial concentrations of Beclin1 and Caspases largely determine whether cells stay in autophagy or apoptosis. Increasing *D* decreases the robustness of the system.

3.3.2. Noise-induced switch from autophagy to apoptosis

In this section, we conduct deterministic and stochastic analyses to explore how both S and k_i $(i = 4, 8)$ affect the transition from autophagy to apoptosis and further influence the fate of cells. Deterministic codimension-1 and -2 bifurcation diagrams are shown in Figure 14. In the codimension-1 bifurcation diagrams, we adjusted the parameters k_4 and k_8, respectively, to observe how the bifurcation curves of $[B]$ and $[C]$ would change with respect to S.

The values of the parameter k_4 decreased from 4 to 2, and then to 0.2 (Figure 14A1,A2), causing the bifurcation curves of $[B]$ and $[C]$ to shift from left to right. Simultaneously, the fold bifurcation point F_2 moved to the right into the positive part of the stress axis, leading to a bistable switch from irreversible to reversible. When $k_4 = 0.2$, the bifurcation curves of $[B]$ and $[C]$ exhibited monostable states for high and low concentrations, respectively. When the values of the parameter k_8 decreased from 0.37 to 0.17 (Figure 14B1,B2), the bifurcation curves of $[B]$ and $[C]$ showed the same trend as that observed for k_4. However, the result for $k_8 = 0.57$ was contrary to that for $k_4 = 0.2$, as the bifurcation curves showed monostable states for low $[B]$ and high $[C]$, respectively.

More globally, the codimension-2 bifurcation analyses in the (S,k_4)- and (S,k_8)-planes are given in Figure 14C1,C2, respectively. The fold bifurcation curves f_1 and f_2 originated from the cusp point, which divides the (S, k_4)- or (S,k_8)-plane into two monostable regions and a bistable region based on the number of stable steady states. In addition, we added three dashed lines in Figure 14C1,C2, respectively, to indicate three different values of k_4 and k_8 in the codimension-1 bifurcation diagrams (Figure 14A1,A2,B1,B2). The codimension-2 bifurcation diagrams displayed more globally the regions of the monostable and bistable steady states.

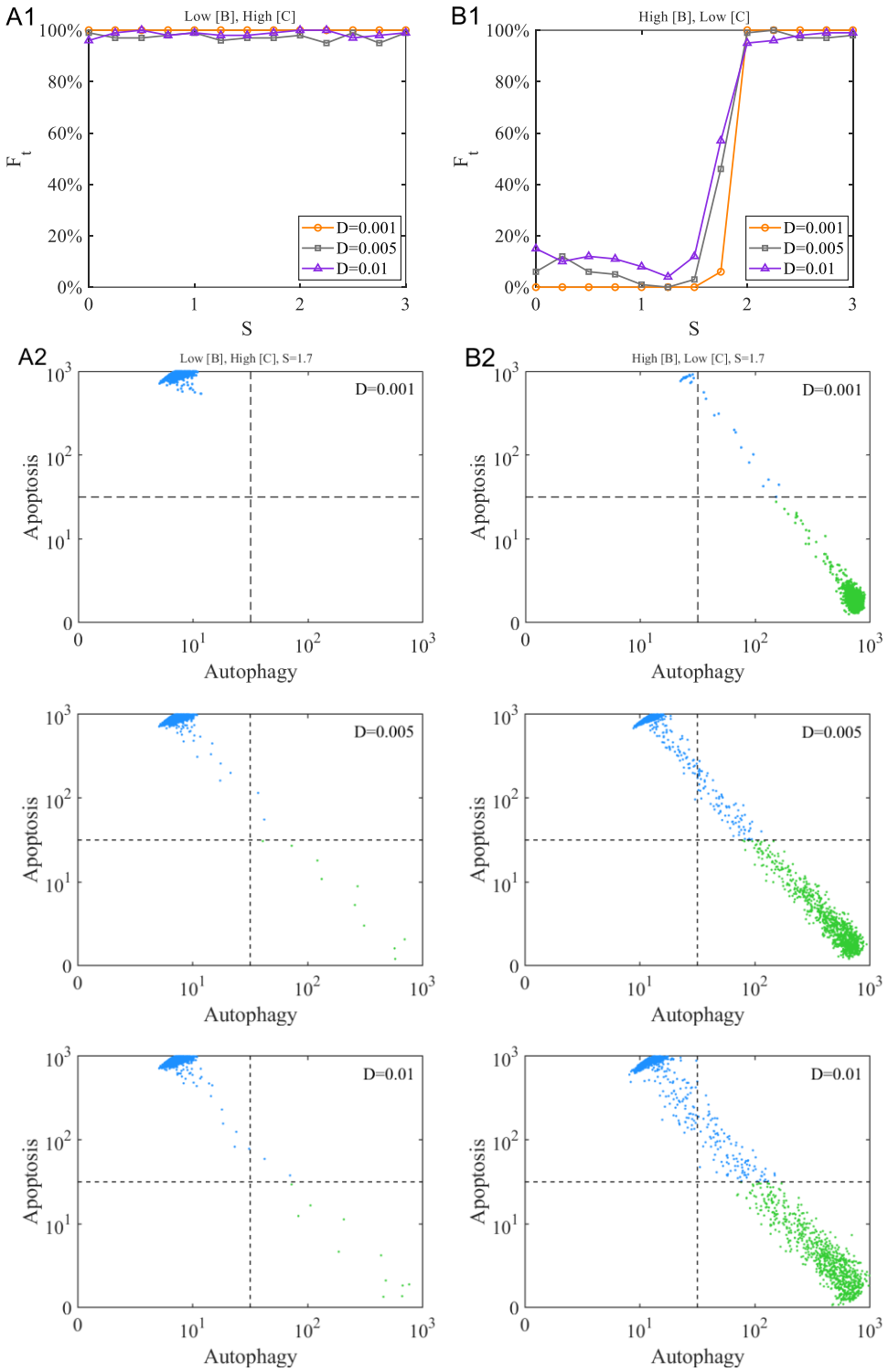

Figure 13. Stochastic behaviors of the cell population with different levels of S under conditions of low Beclin1 but high Caspases (A) and high Caspases but low Beclin1 (B). F_t is the ratio of transiting cells to all cells and as a function of S for different values of D. The scatter plots for each cell for autophagy (green point) or apoptosis (blue point) calculated at $t = 30$ h.

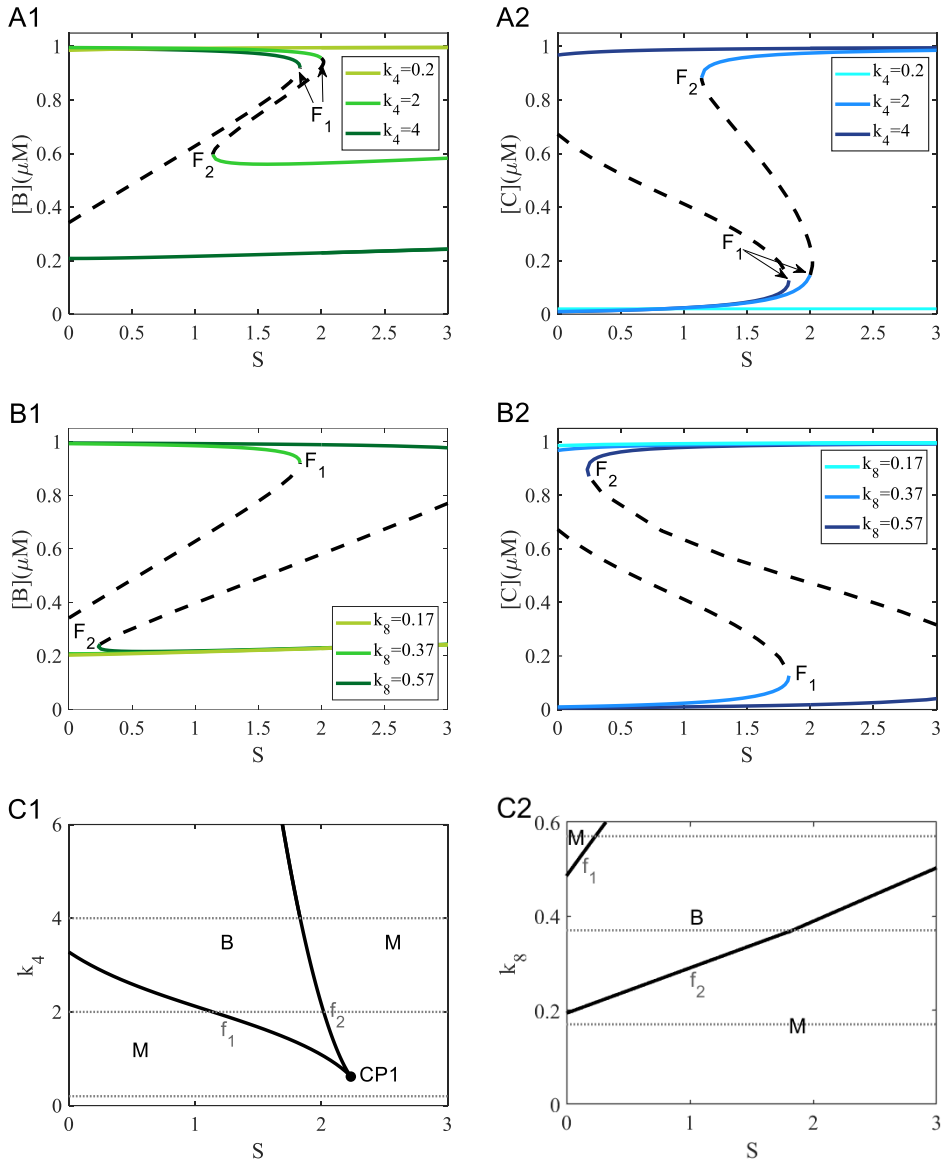

Figure 14. Codimension-1 bifurcation diagrams for Beclin1 and Caspases for different values of k_4 (A) and k_8 (B), and codimension-2 bifurcation planes of (S, k_4) and (S, k_8) (C). M, monostable region; B, bistable region; CP, cusp point.

In the bistable regions, where stochastic switching behavior driven by noise may occur, we computed the F_t functions of the stress S and parameter $k_i (i = 4, 8)$ as independent inputs (Figure 15A,B, respectively). Here, we still focused on the different noise strengths D = 0.001, 0.005, and 0.01 under the two different initial conditions of low $[B]$ but high [C] (Figure 15A1–A3,B1–B3) and high $[B]$ but low [C] (Figure 15A4–A6,B4–B6).

F_t varied from 0 to 100% and is shown with different intensities to reflect the percentage of apoptotic cells. In the planes of (S, k_i) $(i = 4, 8)$, there was a clear dividing line between high (yellow) and low (blue) F_t, consistent with the bistable nature of the bifurcation dynamics. For both k_4 and k_8, the yellow area of F_t was much larger under the condition of low $[B]$ but high $[C]$ than that of high $[B]$ but low $[C]$. Increasing the noise strength D led to more randomness of sharp changes from small to large F_t. The bistable thresholds of continuous change for switching from autophagy to

apoptosis under the influence of noise are precisely presented. The noise strength largely enhanced the stochasticity and uncertainty of these transitions.

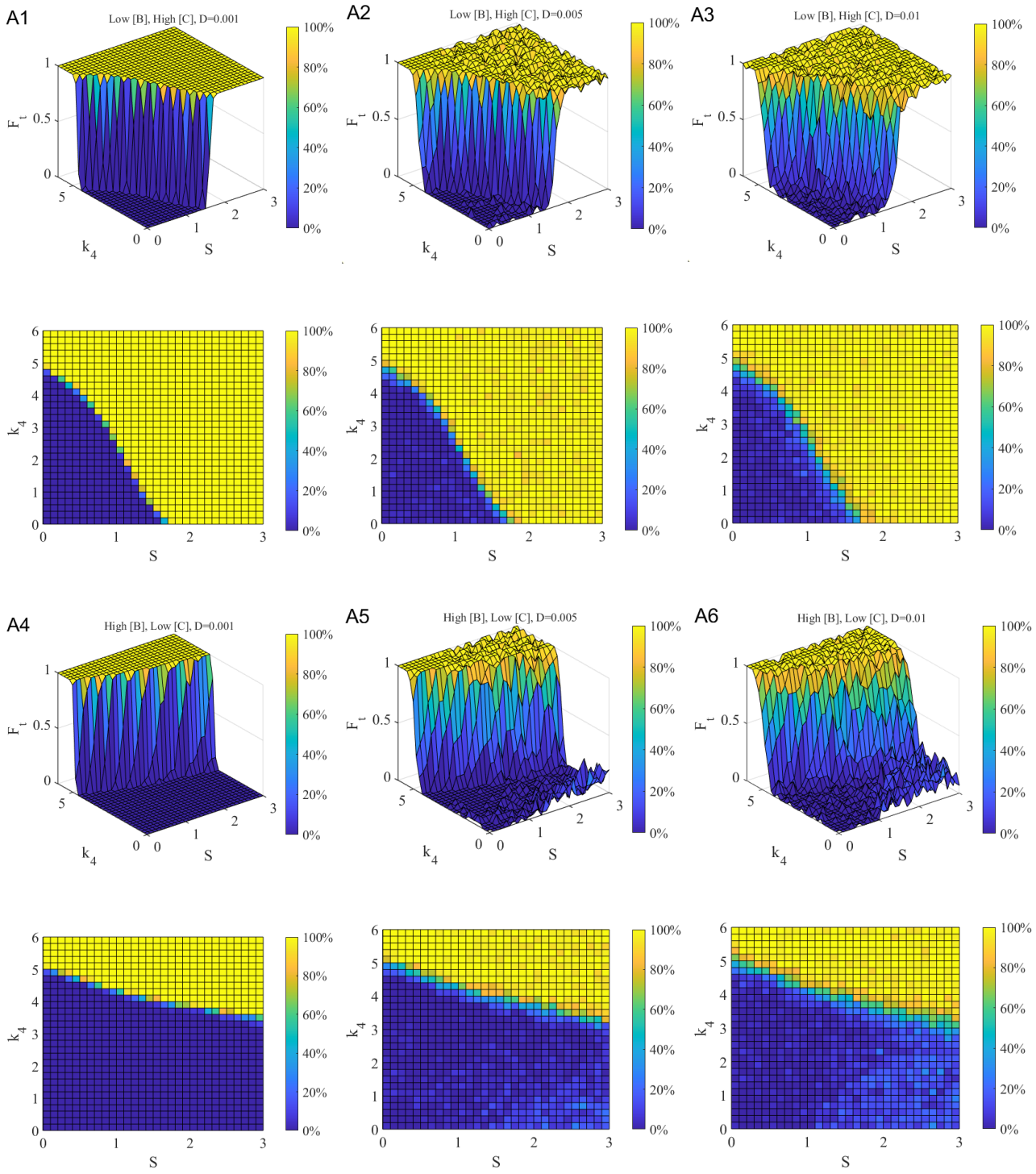

Figure 15. The percentages of apoptotic cells calculated by F_t for stress S and feedback strengths k_4 (A) and k_8 (B) at $t = 30$ h, where $D = 0.001$, 0.005, and 0.01 (from left to right).

Continued on next page

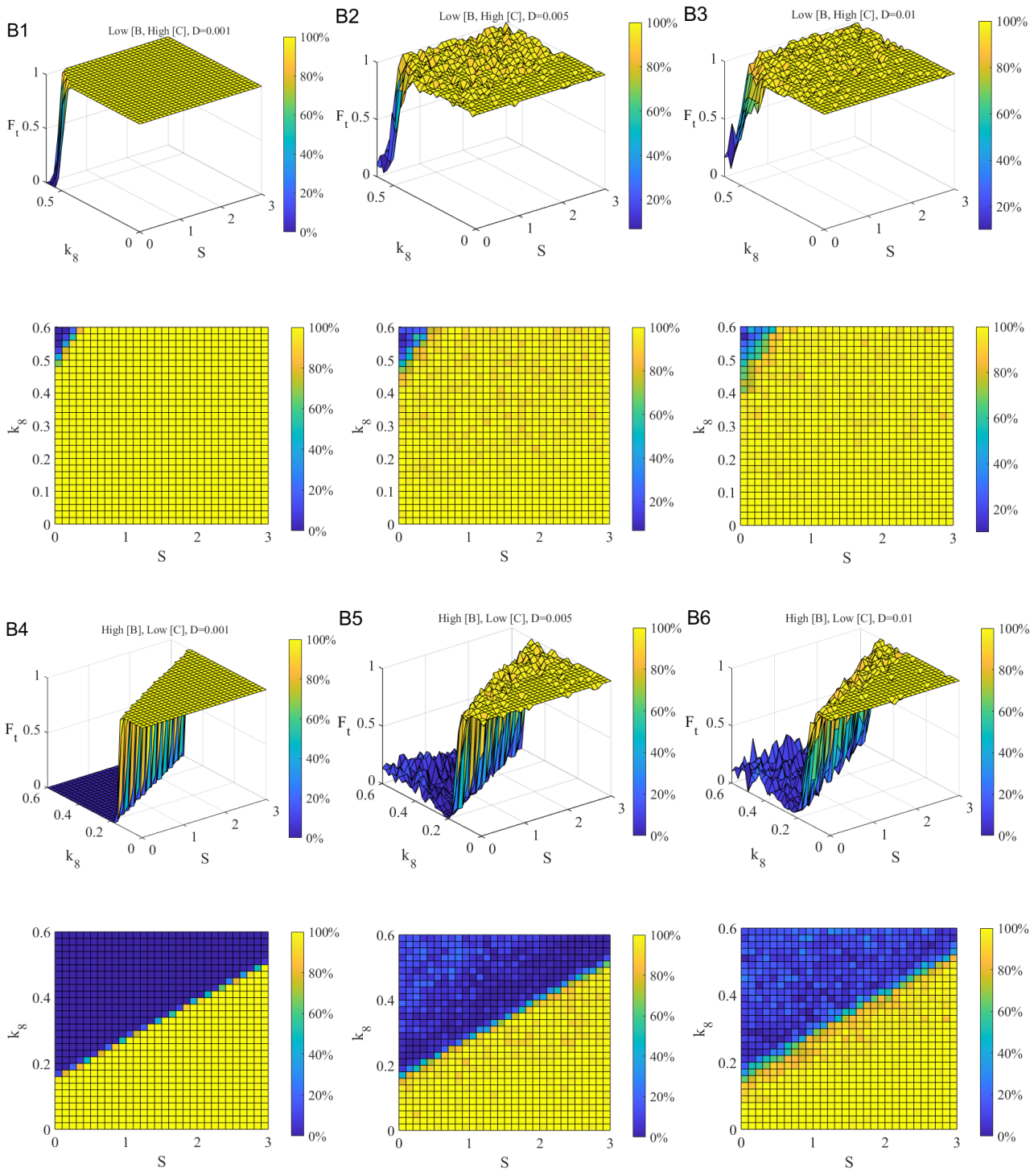

Figure 15. The percentages of apoptotic cells calculated by F_t for stress S and feedback strengths k_4 (A) and k_8 (B) at $t = 30$ h, where $D = 0.001,\ 0.005$, and 0.01 (from left to right).

4. Discussion and conclusions

With the development of molecular biology, the focus of research has gradually shifted from the cellular level to the microscopic exploration of individual proteins [10,26]. We propose a minimal

model by simplifying a mathematical model of stress-directed crosstalk between autophagy and apoptosis consisting of numerous regulatory components and inducers from previous studies [6]. The minimal model contains only two main protein types, Beclin1 and Caspases, to induce autophagy and apoptosis, respectively, under the stimulation of stress. In this study, the dynamical behavior of autophagy and apoptosis is well investigated through bifurcation and stochastic analysis.

For the deterministic model, the dynamic behaviors of Beclin1 and Caspases were analyzed under two different levels of stress (Figure 2). At low stress levels, the system exhibited bistability for either autophagy or apoptosis, whereas at high stress levels it was monostable for apoptosis only. As different stress levels led to different stability properties, we used a deterministic model with added noise to identify the statistical characteristics of autophagy and apoptosis in cells (Figure 3). When the system perturbed by noise had two different initial conditions, the distribution of cells was more concentrated at low stress than at high stress. This indicates that the system is more robust at low stress than at high stress.

Moreover, considering the antagonistic relationships between Beclin1 and Caspases, the double negative feedback loops between autophagy and apoptosis affected by noise under two different levels of stress and initial conditions were studied (Figures 4–11). The results showed that k_4 (the Caspases-dependent inactivation rate constant of Beclin1) and k_8 (the Beclin1-dependent inactivation rate constant of Caspases) had contrary regulatory effects on the switch from autophagy to apoptosis in deciding cellular life and death with different levels of stress. Both of the two parameters ensured the bistable threshold values of the system (Figures 4, 6, 8 and 10). The bistable range of k_4 under small stress was much larger than under large stress, so the cell itself under the low stress with strong inhibition of Caspases preferred to maintain autophagy. However, the opposite results for k_8 made the cell with strong inhibition of Beclin1 more prone to apoptosis. Stochastic simulations showed that under the two different initial conditions, the noise strength D caused more fluctuation in the bistable range for both k_4 and k_8; the larger the value of D, the stronger the disturbance to the F_t (the ratio of the number of apoptotic cells to all 1000 cells) curves (Figures 5, 7, 9 and 11).

Finally, in light of the above considerations, we comprehensively investigated the noise-induced transition from autophagy to apoptosis under continuously varying stress (Figures 12–15). The deterministic bifurcation curves of $[B]$ and $[C]$ indicated that autophagy is initially activated as stress increases, followed by the activation of apoptosis (Figure 12). In the stochastic simulation, the different initial conditions largely determined whether cells stayed in autophagy or apoptosis at a given stress level (Figure 13). Moreover, the robustness of the system decreased as D increased. Owing to significant changes in the codimension-1 bifurcation curves of $[B]$ and $[C]$ with varying k_i $(i = 4, 8)$ in the planes of $(S, [B])$ (or $(S, [C])$), the codimension-2 bifurcations were plotted to illustrate the overall bistable and monostable distributions (Figure 14). The bistable regions, in which stochastic switching was driven by noise, showed that noise strength enhanced the stochasticity of the transition from autophagy to apoptosis (Figure 15).

Autophagy and apoptosis are complex and sophisticated processes in cellular systems. The double negative feedback loops between them largely determines the mechanism of first autophagy and then apoptosis. However, it is difficult and important to guarantee the order of the mechanism under noise. Therefore, we added the Gaussian white noise into the system and the mathematical model obtained several advantages. First, sequence and completeness of autophagy and apoptosis with noise addition were achieved in our model, and the underlying mechanisms were analyzed in detail. Second, the double negative feedback loops in the system exhibited bistability extremely important in cell signaling.

Furthermore, noise perturbations on the double negative feedback loops were useful to analyze the fundamental switching transition from autophagy to apoptosis. Third, in the presence of noise perturbations, the system was more in accordance with the real case and served as a guidance for future studies.

It should be noted that although our model was analyzed with noise, which was at a holistic level, rather than a more detailed aspect of the feedback loops with noise added. In other words, the precise addition of noise terms to stress or the critical parameters of k_4 and k_8 in the double negative feedback loops remains a difficult problem. In addition, it is crucial to consider the addition of noise more reasonably, science the huge number of regulatory components and the complexity of the feedback loops may work together to affect the transition from autophagy to apoptosis. Though the implementation of these results mainly relies on bifurcation analysis and numerical simulations, how to overcome these problems will be a future topic.

The most important difference between our model and other published models [6,26–28] is that we did not consider complex models with more interaction feedback loops. Instead, we aimed to simplify the complex model to gain an essential understanding of the switch from autophagy to apoptosis. The deterministic and stochastic approaches were used to analyze the transition process. The former showed that the bistable phenomenon of the system is the core dynamic behavior of the transition from autophagy to apoptosis. The latter described the stochastic fluctuations induced by noise that trigger the switch and affect the dynamical behavior of the cell population. These findings may shed light on fundamental understanding of the dynamics of the system. Bistable switching is extremely important in cellular signaling, and noise intensity increases the randomness of the switch. Cell population behavior gives a good description of the dynamical properties of the system.

In conclusion, a minimal model of the crosstalk between autophagy and apoptosis has been developed and analyzed in the present study. The mathematical modeling approach used in this study may be beneficial for gaining a system-level understanding of this complex and important mechanism. Our work may provide meaningful insights for future dynamics modeling of autophagy and apoptosis.

Use of AI tools declaration

The authors declare they have not used artificial intelligence (AI) tools in the creation of this article.

Acknowledgements

The authors are grateful to the anonymous referees and editors for their valuable suggestions which helped us to improve the quality of this work. This work was supported by the National Natural Science Foundation of China (12372060).

Conflict of interest

The authors declare that they have no conflict of interest.

References

1. W. Cao, J. Li, K. Yang, D. Cao, An overview of autophagy: Mechanism, regulation and research progress, *Bull. Cancer*, **108** (2021), 304–322. https://doi.org/10.1016/j.bulcan.2020.11.004
2. H. Yamamoto, S. Zhang, N. Mizushima, Autophagy genes in biology and disease, *Nat. Rev. Genet.*, **24** (2023), 382–400. https://doi.org/10.1038/s41576-022-00562-w
3. S. Liu, S. Yao, H. Yang, S. Liu, Y. Wang, Autophagy: Regulator of cell death, *Cell Death Dis.*, **14** (2023), 648. https://doi.org/10.1038/s41419-023-06154-8
4. W. Xie, J. Zhou, Aberrant regulation of autophagy in mammalian diseases, *Biol. Lett.*, **14** (2018), 20170540. https://doi.org/10.1098/rsbl.2017.0540
5. O. Kapuy, B. Lizák, I. Stiller, G. Bánhegyi, A systems biological perspective of cellular stress-directed programmed cell death, *Comput. Mol. Biosci.*, **4** (2014), 28–34. https://doi.org/10.4236/cmb.2014.41003
6. O. Kapuy, P. K. Vinod, J. Mandl, G. Bánhegyi, A cellular stress-directed bistable switch controls the crosstalk between autophagy and apoptosis, *Mol. BioSyst.*, **9** (2013), 296–306. https://doi.org/10.1039/C2MB25261A
7. M. C. Maiuri, E. Zalckvar, A. Kimchi, G. Kroemer, Self-eating and self-killing: crosstalk between autophagy and apoptosis, *Nat. Rev. Mol. Cell Biol.*, **8** (2007), 741–752. https://doi.org/10.1038/nrm2239
8. V. Nikoletopoulou, M. Markaki, K. Palikaras, N. Tavernarakis, Crosstalk between apoptosis, necrosis and autophagy, *Biochim. Biophys. Acta, Mol. Cell Res.*, **1833** (2013), 3448–3459. https://doi.org/10.1016/j.bbamcr.2013.06.001
9. M. Redza-Dutordoir, D. A. Averill-Bates, Activation of apoptosis signalling pathways by reactive oxygen species, *Biochim. Biophys. Acta, Mol. Cell Res.*, **1863** (2016), 2977–2992. https://doi.org/10.1016/j.bbamcr.2016.09.012
10. L. A. Booth, S. Tavallai, H. A. Hamed, N. Cruickshanks, P. Dent, The role of cell signalling in the crosstalk between autophagy and apoptosis, *Cell. Signalling*, **26** (2014), 549–555. https://doi.org/10.1016/j.cellsig.2013.11.028
11. K. Cadwell, Crosstalk between autophagy and inflammatory signalling pathways: balancing defence and homeostasis, *Nat. Rev. Immunol.*, **16** (2016), 661–675. https://doi.org/10.1038/nri.2016.100
12. K. F. Cooper, Till death do us part: The marriage of autophagy and apoptosis, *Oxid. Med. Cell Longevity*, **2018** (2018), 1-13. https://doi.org/10.1155/2018/4701275
13. J. Doherty, E.H. Baehrecke, Life, death and autophagy, Nat, *Cell Biol*. **20** (2018), 1110–1117. https://doi.org/10.1038/s41556-018-0201-5
14. C. Gordy, Y. W. He, The crosstalk between autophagy and apoptosis: where does this lead, *Protein. Cell*, **3** (2012), 17-27. https://doi.org/10.1007/s13238-011-1127-x
15. R. Kang, H. J. Zeh, M. T. Lotze, D. Tang, The Beclin 1 network regulates autophagy and apoptosis, *Cell Death Differ.*, **18** (2011), 571–580. https://doi.org/10.1038/cdd.2010.191
16. F. Strappazzon, M. Vietri-Rudan, S. Campello, F. Nazio, F. Florenzano, G.M. Fimia, et al., Mitochondrial BCL-2 inhibits AMBRA1-induced autophagy, *EMBO J.*, **30** (2011), 1195–1208. https://doi.org/10.1038/emboj.2011.49
17. S. Song, J. Tan, Y. Miao, M. Li, Q. Zhang, Crosstalk of autophagy and apoptosis: Involvement of the dual role of autophagy under ER stress, *J. Cell Physiol.*, **232** (2017), 2977–2984. https://doi.org/10.1002/jcp.25785

18. T. T. Su, Cellular plasticity, caspases and autophagy; that which does not kill us, well, makes us different, *Open Biol.*, **8** (2018), 180157. https://doi.org/10.1098/rsob.180157
19. A. B. Uzdensky, Apoptosis regulation in the penumbra after ischemic stroke: expression of pro- and antiapoptotic proteins, *Apoptosis*, **24** (2019), 687–702. https://doi.org/10.1007/s10495-019-01556-6
20. A. Ashkenazi, W. J. Fairbrother, J. D. Leverson, A. J. Souers, From basic apoptosis discoveries to advanced selective BCL-2 family inhibitors, *Nat. Rev. Drug Discovery*, **16** (2017), 273–284. https://doi.org/10.1038/nrd.2016.253
21. R. Singh, A. Letai, K. Sarosiek, Regulation of apoptosis in health and disease: the balancing act of BCL-2 family proteins, *Nat. Rev. Mol. Cell Biol.*, **20** (2019), 175–193. https://doi.org/10.1038/s41580-018-0089-8
22. Z. Li, M. Ni, J. Li, Y. Zhang, Q. Ouyang, C. Tang, Decision making of the p53 network: Death by integration, *J. Theor. Biol.*, **271** (2011), 205-211. https://doi.org/10.1016/j.jtbi.2010.11.041
23. R. Ma, D. Yu, Y. Peng, H. Yi, Y. Wang, T. Cheng, et al., Resveratrol induces AMPK and mTOR signaling inhibition-mediated autophagy and apoptosis in multiple myeloma cells, *Acta Biochim. Biophys. Sin.*, **53** (2021), 775–783. https://doi.org/10.1093/abbs/gmab042
24. G. Y. Liu, W. L. Xie, Y. T. Wang, L. Chen, Z. Z. Xu, Y. Lv, et al., Calpain: the regulatory point of myocardial ischemia-reperfusion injury, *Front. Cardiovasc. Med.*, **10** (2023), 1194402. https://doi.org/10.3389/fcvm.2023.1194402
25. E. Kania, G. Roest, T. Vervliet, J. B. Parys, G. Bultynck, IP3 receptor-mediated calcium signaling and its role in autophagy in cancer, *Front. Oncol.*, **7** (2017), 140. https://doi.org/10.3389/fonc.2017.00140
26. B. Liu, Z. N. Oltvai, H. Bayır, G. A. Silverman, S. C. Pak, D. H. Perlmutter, et al., Quantitative assessment of cell fate decision between autophagy and apoptosis, *Sci. Rep.*, **7** (2017), 17605. https://doi.org/10.1038/s41598-017-18001-w
27. I. Tavassoly, J. Parmar, A. N. Shajahan-Haq, R. Clarke, W. T. Baumann, J. J. Tyson, Dynamic modeling of the interaction between autophagy and apoptosis in mammalian cells, *CPT Pharmacometrics Syst. Pharmacol.*, **4** (2015), 263-272. https://doi.org/10.1002/psp4.29
28. B. J. Yang, Q. S. Liu, Y. H. Bi, Autophagy and apoptosis are regulated by stress on Bcl2 by AMBRA1 in the endoplasmic reticulum and mitochondria, *Theor. Biol. Med. Modell.*, **16** (2019), 18. https://doi.org/10.1186/s12976-019-0113-5
29. M. Holczer, M. Márton, A. Kurucz, G. Bánhegyi, O. Kapuy, A comprehensive systems biological study of autophagy-apoptosis crosstalk during endoplasmic reticulum stress, *BioMed. Res. Int.*, **2015** (2015), 319589. https://doi.org/10.1155/2015/319589
30. O. Kapuy, P. K. Vinod, G. Bánhegyi, mTOR inhibition increases cell viability via autophagy induction during endoplasmic reticulum stress—An experimental and modeling study, *FEBS. Open Bio*, **4** (2014), 704–713. https://doi.org/10.1016/j.fob.2014.07.006
31. P. Smolen, D. A. Baxter, J. H. Byrne, Interlinked dual-time feedback loops can enhance robustness to stochasticity and persistence of memory, *Phys. Rev. E*, **79** (2009), 031902. https://doi.org/10.1103/PhysRevE.79.031902
32. J. Tang, X. Yang, J. Ma, Y. Jia, Noise effect on persistence of memory in a positive-feedback gene regulatory circuit, *Phys. Rev. E*, **80** (2009), 011907. https://doi.org/10.1103/PhysRevE.80.011907
33. X. P. Zhang, Z. Cheng, F. Liu, W. Wang, Linking fast and slow positive feedback loops creates an optimal bistable switch in cell signaling, *Phys. Rev. E*, **76** (2007), 031924. https://doi.org/10.1103/PhysRevE.76.031924

34. M. Chen, L. Wang, C. C. Liu, Q. Nie, Noise attenuation in the ON and OFF states of biological Switches, *ACS Synth. Biol.*, **2** (2013), 587–593. https://doi.org/10.1021/sb400044g
35. V. Hatzimanikatis, C. Gérard, D. Gonze, F. Lemaigre, B. Novák, A model for the epigenetic switch linking inflammation to cell transformation: deterministic and stochastic approaches, *PLoS Comput. Biol.*, **10** (2014), e1003455. https://doi.org/10.1371/journal.pcbi.1003455
36. B. Ermentrout, Simulating, analyzing, and animating dynamical systems: a guide to XPPAUT for researchers and students, *Appl. Mech. Rev.*, (2002). https://doi.org/10.1137/1.9780898718195
37. A. Dhooge, W. Govaerts, Y. A. Kuznetsov, MATCONT: a matlab package for numerical bifurcation analysis of ODEs, *ACM Trans. Math. Softw*, **29** (2003), 141–164. https://doi.org/10.1145/779359.779362

AIMS Press